DYNAMIC RESPONSE CHARACTERISTICS OF A CIRCULATION CONTROL ROTOR MODEL PNEUMATIC SYSTEM

Charles B. Watkins
Professor
Howard University
Washington, D.C.

Kenneth R. Reader
Senior Aerospace Engineer
David W. Taylor Naval Ship Research
and Development Center
Bethesda, MD

and

Subash K. Dutta
Graduate Assistant
Howard University
Washington, D.C.

Abstract

Numerical and experimental simulation of unsteady airflow through the control valve and slotted air duct of a circulation control rotor is described. The numerical analysis involves the solution of the quasi-one-dimensional compressible fluid-dynamic equations in the blade air duct together with the coupled isentropic flow equations for flow into the blade through the valve and out of the blade through the Coanda slot. Numerical solutions are compared with basic experimental results obtained for a mockup of a circulation control rotor and its pneumatic valving system. The pneumodynamic phenomena that were observed are discussed with particular emphasis on the characteristic system time lags associated with the response of the flow variables to transient and periodic control valve inputs.

Notation

A	Cross-sectional area of duct
A_e	Effective expansion area at valve exit
A_v	Valve area
f	Duct friction factor
C_s	Slot discharge coefficient
C_v	Valve discharge coefficient
c_v	Specific heat at constant volume
D_h	Hydraulic diameter of duct
e	Total energy per unit volume
F	Flux times area vector
G	Vector of nonhomogeneous terms in flow equations
h	Heat transfer coefficient
H_D	Average duct height
k	Thermal conductivity
L	Length of duct
$\dot{m}$	Mass flow rate
m	Mass flow rate per unit area in duct
m_I	Mass flow rate per unit area computed from isentropic flow theory
m_s	Mass flow rate per unit area through slot
m_v	Mass flow rate per unit area through valve
p	Static pressure in duct
p_{ext}	External pressure at slot exit
p_0	Total pressure in duct
T	Duct static temperature
T_0	Duct total temperature
T_w	Duct wall temperature
t	Time
U	Vector of dependent variables
V	Vector of diffusion terms
v_x	Average duct velocity in spanwise or x direction
v_y	Approximate average duct velocity in chordwise or y direction
w_s	Slot width
x	Spanwise coordinate
x_e	Coordinate at duct entrance

x_{end}	Coordinate at duct end
y	Chordwise coordinate
γ	Ratio of specific heats
ρ	Density
ω	Angular frequency

Subscripts

I	Variable computed from isentropic flow at valve exit
pl	Variable in pressure supply plenum or rotor hub

Prefix

Peak-to-peak value of variable

Introduction

Circulation control rotor (CC) technology applied to rotary-wing aircraft or stopped-rotor vertical takeoff and landing (VTOL) aircraft, such as the X-Wing, offers several distinct advantages over conventional rotor technology. For rotary-wing aircraft, CC technology provides a solution to such problems as high vibration levels, retreating blade stall, hub/pylon drag, and implementing higher harmonic control. For stopped-rotor aircraft, the historical limitations of aeroelastic divergence, flutter, blade dynamic instability, and critical resonance conditions during rpm reduction are eliminated. Both types of aircraft use a shaft-driven rotor with blades having circulation control airfoils which generate lift through the Coanda principle. The CC airfoils employ a rounded trailing edge with a thin jet of air tangentially ejected from a spanwise slot adjacent to the rounded (Coanda) surface. The jet of air suppresses boundary layer separation and moves the rear stagnation streamline toward the lower surface, thereby increasing lift. Lift is increased in proportion to the mass flow rate of compressed air in the jet. Pitch and roll control requirements are obtained by cyclic modulation of the mass flow rate with valves in the nonrotating system. Higher harmonic cyclic control can be similarly applied for reducing blade stresses, transmitted shears, vibration, and power requirements.

The design of CC rotors and their pneumatic control systems requires an understanding and appreciation of the phenomenology involved in the control and distribution of airflow to the Coanda slots in these rotors. A capability for analytical prediction of rotor Coanda airflow is also essential. The term "pneumodynamics" has been coined to refer to the aerodynamic response characteristics of CC rotor system internal airflow.

In a recent paper, Watkins et al.[1] describe the modeling techniques employed in the HFPA (high frequency pneumodynamic analysis) computer code developed for CC rotor pneumodynamic analysis. The present paper reviews the modeling techniques described in Reference 1 and presents results obtained by applying the code to a simple experimental mockup of a model rotor blade and its pneumatic valving system. The discussion of the results, from both the HFPA predictions and the experiment, focuses on the dynamic response of the flow variables to periodic and transient control valve inputs. These response characteristics, particularly with reference to the characteristic system time lags, have implications for the performance of actual rotor systems.

Theory

The modeling techniques employed in the present research are described in Reference 1 where emphasis is on the details of the theoretical formulation and numerical technique. The theory is presented here in abbreviated form; a more complete discussion is contained in Reference 1.

Basic Equations

The HFPA code solves the quasi-one dimensional, compressible fluid dynamic equations for unsteady flow in a spanwise blowing air supply duct internal to a rotating CC rotor blade, together with the coupled isentropic flow equations for flow into the blade through the control valve and out of the blade through the Coanda slot. The duct flow equations have the conservative form representation

$$U_{,t} + \frac{1}{A} F_{,x} + G + V = 0 \qquad (1)$$

where the vector of dependent variables is

$$U = \begin{bmatrix} \rho \\ m \\ e \end{bmatrix}$$

and the flux is given by

$$F = \begin{bmatrix} mA \\ \left(\frac{m^2}{\rho} + p\right) A \\ (e + p) \frac{m}{\rho} A \end{bmatrix}$$

The vector of nonhomogeneous terms, which includes the effects of blade rotation at angular velocity ω, wall skin friction factor $c_f(x)$, wall heat transfer coefficient $h(x)$, and mass flux through the slot $m_s(x,t)$ is

$$G = \begin{bmatrix} \frac{m_s w_s}{A} \\ -\frac{p}{A}\frac{dA}{dx} + \frac{m_s w_s m}{\rho A} + \frac{2c_f m^2}{D_H \rho} - \rho\omega^2 x \\ \frac{m_s w_s (e+p)}{A\rho} - m\omega^2 x + \frac{4h}{D_H}(T - T_w) \end{bmatrix}$$

For completeness, the vector of axial diffusion terms is included, although it is insignificant in the present problem. It is

$$V = \begin{bmatrix} 0 \\ \frac{4}{3}\left(\frac{m}{\rho}\right)_{,xx} \\ -\frac{4}{3}\left[\frac{m}{\rho}\left(\frac{m}{\rho}\right)_{,x}\right]_{,x} - kT_{,xx} \end{bmatrix}$$

The equation of state is

$$p = (\gamma-1)\left(e - \frac{m^2}{2\rho} - \rho\,\frac{v_y^2}{2}\right) \qquad (2)$$

In the above relations, the conservative variables m and e are defined as

$$m = \rho v_x$$

$$e = \rho\left(c_v T + \frac{v_x^2}{2} + \frac{v_y^2}{2}\right)$$

and $w_s(x,t)$ and $m_s(x,t)$ are the local (with respect to spanwise x location) slot width and blowing mass flux, respectively.

The small average chordwise velocity component inside the duct can be crudely approximated as

$$v_y \simeq \frac{w_s m_s}{2\rho H_D} \qquad (3)$$

in which $H_D(x)$ is the local effective height of the duct.

The mass flux distribution through the Coanda slot is assumed to be well represented by one-dimensional isentropic flow theory with a discharge coefficient $C_s(x)$;

$$m_s(x,t) = C_s m_I(p_0, T_0, p_{ext}) \qquad (4)$$

The above functional relationship is the usual expression for isentropic flow expanding through a nozzle from a plenum (in this case the duct interior) to ambient conditions (in this case the exterior of the rotor blade). $p_0(x,t)$ and $T_0(x,t)$ are the local (internal) total pressure and temperature, respectively, and $p_{ext}(x,t)$ is the external pressure at the exit of the Coanda slot. Dependency upon external pressure is eliminated when the flow is choked.

Boundary Conditions

At the upstream boundary $x = x_e$, a plenum supplies blowing air to the duct through a valving system. The valve opening area has constant and rotor-azimuth-dependent components regulated by the collective and cyclic components, respectively, of the aircraft control system. The mass flow and duct pressures are thus determined by these valve settings in concert with the duct/slot configuration.

Figure 1 shows the idealized representation adopted for the cam type valve of interest in the present study. The controlled value of the valve opening is designated as $A_v(t)$, and A_e is the fixed effective opening at the duct entrance. Like the slot flow, one-dimensional isentropic flow theory with a discharge coefficient is used to represent flow through the valve. The valve mass flux is

$$m_v(t) = C_v m_I(p_{0_{pl}}, T_{0_{pl}}, p(x_e,t)) \qquad (5)$$

where p_0 and T_0 are the total pressure and temperature, respectively, in the air supply plenum in the rotor hub and $p(x_e,t)$ is the back pressure in the duct entrance downstream of the valve. When the flow is choked, the dependency on $p(x_e,t)$ is eliminated.

The other boundary condition, at $x=x_{end}$, is the stagnation of the flow at the end of the duct.

The discharge coefficients C_v and C_s, used as correlation parameters for a given system relate the geometric area of a system to the effective area. For simple configurations such as orifice plates or venturi tubes in a well conditioned system where the airflow is well behaved, the discharge coefficient value can be obtained from a standard engineering handbook.

Finite Difference Method

In applying the theory of the previous section to the analysis of a rotor blade, the entire blade, including the transition duct (ducting from hub valve exit to airfoil portion of rotor blade), is discretized by dividing it into spanwise (radial) segments. The governing differential equations, Eq. (1), are solved by the implicit, "delta form," finite-difference procedure of Beam and Warming[2] at the grid points located at segment boundaries, including the valve exit as shown in Fig. 1 and the duct end. The solution of the duct flow is actively coupled to the flow through the valve and through the upstream boundary condition. With the exception of the upstream boundary condition for flow into the duct from the valve, the numerical analysis is rather standard and is described fully in Reference 1.

In Reference 1, expressions are presented for an approximate numerical upstream boundary condition based on deriving for various valve types an auxiliary relationship by ignoring the time dependent term in the momentum equation between the first two grid points (grid point 1 and 2 in Fig. 1). The approximation for the idealized valve of Fig. 1 is

$$p_1 A_e + \frac{(p_1+p_2)}{2}(A_2-A_e) = \frac{m_2^2}{\rho_2} A_2 + p_2 A_2 + \frac{(A_e-A_2)\rho_2\omega^2}{4}(x_1^2-x_2^2) - 2\frac{C_f m_2^2}{\rho_2 D_H}(x_1-x_2) \qquad (6)$$

Approximations such as in Eq. (6) were applied because the investigators were unsuccessful in applying the more standard, and less approximate, procedures for inlet boundary conditions of applying

one-sided differencing or the method of characteristics. The presence of the valve poses special difficulties in the application of these standard techniques. In a recent communication, Anderson of United Technologies Research Center indicated that he was successful in applying the method of characteristics to derive inlet boundary conditions for the HFPA code for a sudden expansion or gate-type valve. The extension of his procedure to the cam valve type shown in Fig. 1, is not straightforward due to the 90 deg change in flow direction. Since this valve is the type considered in the present investigation, Eq. (6) was retained.

Numerical Solution Procedure

The basic approach followed in obtaining numerical solutions to control inputs, consisting of constant (collective) settings or constant collective settings with superimposed constant amplitude cyclic inputs, is to obtain the steady state or time periodic solutions by allowing them to evolve from a transient.

The solution starts with the system essentially at supply pressure conditions. The initial valve position is assumed to be fully open as specified by the sum of its Fourier components supplied as input. The solution is then advanced with time as the flow in the blade adjusts itself to reach steady state flow conditions for the fully open valve. If cyclic components are to be considered, the cyclic input is imposed after fully open steady state flow conditions are achieved. The solution is thereafter advanced further with time until periodic conditions are attained. A harmonic analysis of pressures, temperatures, and mass flow rates is performed on the results from the final cycle.

Experiment

The analytical formulation and the numerical methods described in the previous sections were validated by applying them to a basic experiment and comparing the results with the experimental data[3]. The experiment was performed using a mock-up of a rotor blade pneumodynamic system incorporating a valve similar to the idealized valve of Fig. 1. The model consisted of a supply plenum and two rotating cams with different profiles mounted on the same shaft allowing either a one-per-rev or two-per-rev profile to be selected by axially positioning the cams on the shaft. The flow was modulated by means of the cams from the plenum through a single nozzle into a stationary plugged pipe with a slot.

The pipe with a full-length slot represented a subscale circulation control rotor blade. The experiment was originally performed[3] to establish the feasibility of modulating the weight flow in a one-per-rev and two-per-rev manner and to show that the three components of the airflow were additive. For simplicity, the correct relative motion was established by interchanging the rotating and non-rotating components. The plenum and pipe (hub and rotor blade) were stationary, and the cams (the valving system) rotated. The pipe incorporated several pressure taps distributed along its length. The model is shown in Fig. 2, which is reproduced from Reference 1.

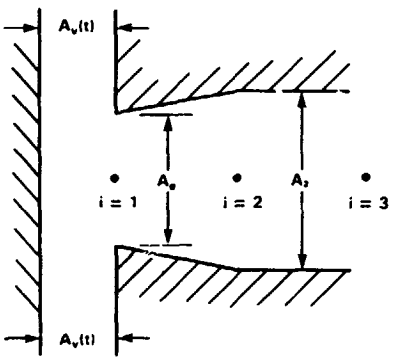

Fig. 1 Idealized valve

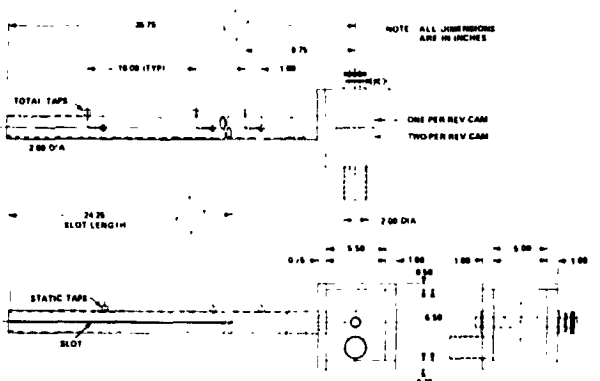

Fig. 2 Experimental model

Dynamic measurements of pipe pressure were obtained for a range of cam rotational speeds. In addition, quasi-dynamic results were obtained by positioning the cam at discrete increments of 30 deg. Average mass flow data were collected from a venturi tube located upstream of the plenum.

Figure 3, also from Reference 1, shows the measured valve area formed by the one-per-rev and two-per-rev cams spaced at a minimum distance of 0.01 in from the nozzle inlet. The points shown were calculated from the measured gap between the cam profile and the nozzle; the area variations are intended to approximate sinusoids as shown. The two-per-rev cam profile is a rather crude approximation and contains a significant higher harmonic content. The measured values were used in the numerical predictions.

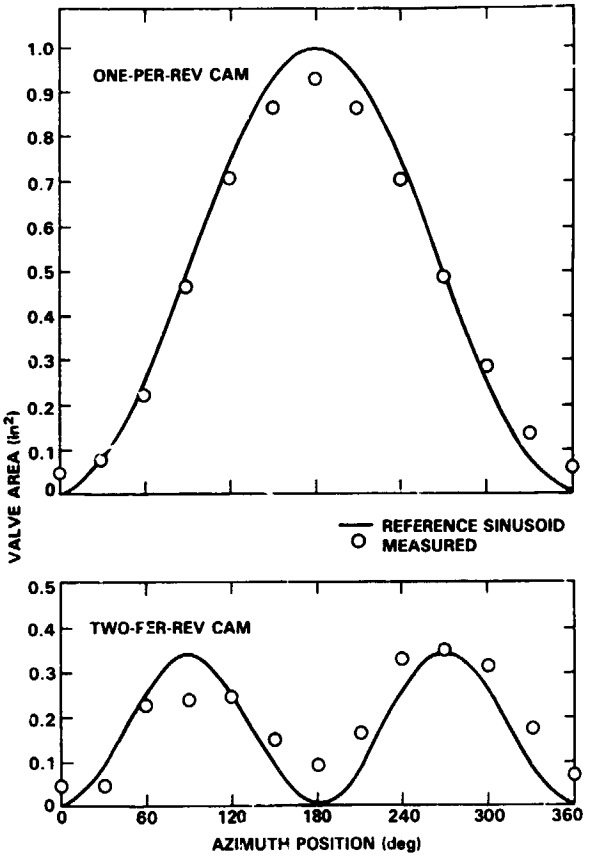

Fig. 3 Valve control area

Results and Discussion

Numerical results were obtained for the experimental configuration of Fig. 2 by discretizing the pipe into 16 segments of approximately equal length. The pipe was assumed to be adiabatic, and the friction coefficient was represented by the formulas for fully developed flow. The integration time-step for the calculations simulating the quasi-dynamic experiments was 5×10^{-4} sec. For the dynamic calculations, valve cycling was imposed after an elapsed time of 0.25 sec. and the time-step was reduced to 1200 steps per revolution thereafter. In general, the results were qualitatively similar for the one- and two-per-rev cams. Therefore, the results presented here are, with one exception, for the one-per-rev cam.

Typical quasi-dynamic numerical and experimental results, indicating the dependency of mass flow rates on nozzle control area at a constant slot height of 0.042 in., are displayed for the one-per-rev cam in Fig. 4. In this figure, the mass flow rate is presented as a function of total valve area at a set plenum pressure. As the valve area increases, the data show that mass flow rate tends toward a constant value, indicating that the flow has become controlled by the slot opening.

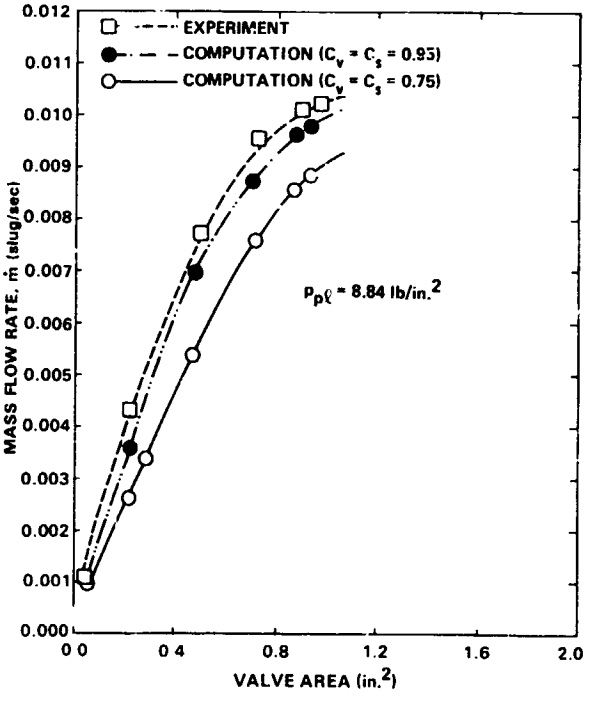

Fig. 4 Mass flow variation

Mass Flow and Pressure Comparison

Figure 4 shows the sensitivity of the discharge coefficients C_v and C_s for a wide range of valve areas. Also shown is the effect of assuming constant values of 0.95 and 0.75 for both the valve and slot discharge coefficients in the numerical solution. The results obtained for the higher value $C_v = C_s = 0.95$ agree more favorably with the experimental results, although the lower discharge coefficient is likely to be realistic physically. That a concept as simple as a discharge coefficient can be used to correlate the mass flow and pressure losses is very encouraging; this is discussed in depth in Reference 4. For the remainder of the theoretical results $C_v = C_s = 0.95$ were used without trying for a better correlation. As indicated in Reference 1, strict interpretation of C_v and C_s is probably not desirable since the various deficiencies and approximations in the computer model can, to some degree, be absorbed by adjusting them. Moreover, the concept of a constant nozzle discharge coefficient is only a first approximation for the actual flow losses which occur over a range of mass flow rates in the analysis. Recent experience with the HFPA code indicates that more physically realistic discharge coefficients can be obtained at the expense of decreased resolution of wave reflection phenomena by including second-order numerical damping in the HFPA algorithm.

Figure 5 illustrates the numerical and experimental cyclic variation of total pressure for a typical dynamic case. The numerical results of Fig. 5 were obtained with $C_v = C_s = 0.95$. The numerically computed pressure profiles have an

azimuthal phase lag from the valve area profiles of Fig. 3 of an approximately 35 deg phase shift. For this configuration, the phase shift is principally due to the finite speed of wave propogation, and is referred to as "sonic lag." A smaller portion of the delay is due to the "capacitance lag" effect caused by the finite pipe volume. The phase difference between the valve area setting and the pressure response to it has been eliminated from Fig. 5 because the experimental phase angle results were not accurate.

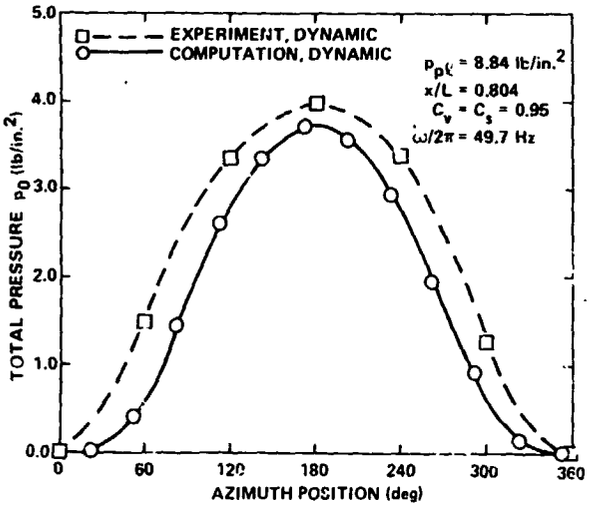

Fig. 5 Total pressure variation

Table 1 contains data obtained from a harmonic analysis of the dynamic numerical results of the case for which the pressures are plotted in Fig. 5. The numerical phase lag has been retained. A harmonic analysis of the experimental pressure data obtained from the experimental curve presented in Fig. 5 is also shown for comparison. Magnitude and phase for the valve opening area, total mass flow rate, and total pressures at two locations are given from the numerical results where the phases are referred to the maximum valve opening at zero deg. (The experimental pressure phase shifts given in the table have an arbitrary reference). The magnitudes are all normalized with respect to the peak-to-peak values.

Table 1 shows that the summation of the higher harmonic content of the mass flow rate output is a rather significant 20 percent while the one-per-rev valve control input contains only approximately 10 percent. Therefore, the mass flow exhibits some nonlinear amplification. The higher harmonic content of the pressure response does not exhibit similar amplification.

The phase shift phenomenon is clearly illustrated by the data in the table. The first harmonic of the mass flow rate lags the valve opening by 39 deg. The first harmonic pressure at, x/L = 0.524, lags the valve opening by 36 deg. At x/L = 0.804, this lag increases to 42 deg. due to the finite wave propogation speed or sonic lag. Because of the specification of a zero numerical integration dissipation parameter in the numerical algorithm used for the cyclic calculations, computed results contain slight, stable spatial numerical oscillations which make it difficult to place confidence in the exact amount of the lag in pressure predicted between locations. Based on the speed of sound, the pure sonic lag between the two points shown should amount to only about one-half the lag shown. The remaining lag may be due to a physical phenomenon or to numerical uncertainty. Although, as discussed previously, the problem of spatial oscillations can be reduced by employing numerical damping, this damping suppresses multiple wave reflections and renders the code less able to predict resonance phenomena. Fortunately, the computed mass flow rate is the result of a spatial integration which has the effect of smoothing the spatial oscillations and should be fairly accurate.

Peak-to-Peak Pressure Comparison

Figure 6 summarizes the results from the dynamic calculations in the form of peak-to-peak total pressures versus frequency for the one-per-rev cam.

Table 1. Harmonic analysis of typical results

HARMONIC n	$A_n/\delta A$ (δA=0.8904 IN^2) MAG(PHASE,DEG)	$\dot{m}_n/\delta\dot{m}$ ($\delta\dot{m}$=0.00331 SLUG/SEC) MAG(PHASE,DEG)	$p_{0n}/\delta p_0$ At x/L = 0.804 COMPUTATION δp_0=3.71 LB/IN^2 MAG(PHASE,DEG)	$p_{0n}/\delta p_0$ At x/L = 0.804 EXPERIMENT δp_0=3.99 LB/IN^2 (APPROXIMATE) MAG(PHASE,DEG)	$p_{0n}/\delta p_0$ At x/L = 0.524 COMPUTATION δp_0=3.77 LB/IN^2 MAG(PHASE,DEG)	$p_{0n}/\delta p_0$ At x/L = 0.524 EXPERIMENT δp_0=3.75 LB/IN^2 (APPROXIMATE) MAG(PHASE,DEG)
0	0.514	0.686	0.425	0.519	0.432	0.537
1	0.509 (353)	0.488 (32)	0.529 (35)	0.494 (350)	0.523 (29)	0.500 (350)
2	0.027 (197)	0.086 (241)	0.016 (55)	0.034 (176)	0.017 (131)	0.043 (171)
3	0.015 (128)	0.014 (100)	0.031 (262)	0.019 (205)	0.007 (275)	0.021 (203)
4	0.006 (26)	0.005 (21)	0 002 (179)	0.007 15)	0.003 (78)	0.005 (45)
5	0.004 (322)	0.002 (63)	0.002 (179)	0.011 (347)	0.003 (346)	0.007 (30)

NOTE: $\omega/2\pi$ = 49.7 Hz AND p_{pl} = 8.89 LB/IN^2.

In Fig. 6 the numerical solution is able to predict fairly well the trends and magnitudes of the pressure response. One possible source of error in the numerical calculations is the assumption of constant discharge coefficient for the wide range of area variation. Somewhat more remote are the possibilities for experimental error.

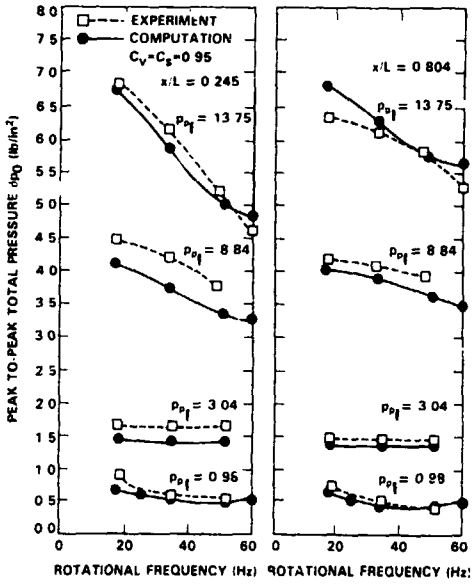

Fig. 6 Peak-to-peak total pressure

Figure 7 plots the dynamic results of the peak-to-peak total pressure near the beginning of the slotted portion of the pipe against plenum pressure for the one-per-rev cam at two different frequencies. The agreement between the measured and numerical results in this figure, in general, is seen to be fair. As shown, the peak-to-peak total pressure at the entrance of the pipe is dependent on the frequency of rotation of the cam. The data shows a droop in the peak-to-peak value of pressure at high plenum pressure and high frequencies; these trends with plenum pressure and frequency are predicted by the computer code. The peak-to-peak total pressure at the entrance of the pipe is shown to be dependent upon the frequency of rotation of the cam.

Figure 8 displays the peak-to-peak static presures versus rotational frequency for various plenum pressures for the one-per-rev cam. The experimental and numerical curves generally show good agreement and the computer code predicts the trends.

Figures 9 and 10 are plots of the ratio of pipe end-to-entrance pressure versus cam rotational frequency for both cams. The two-per-rev cam results are included since the two-per-rev cam extends the frequency range two-fold. Results are

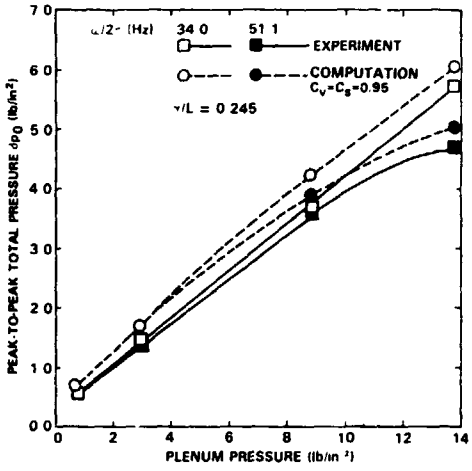

Fig. 7 Effect of plenum pressure

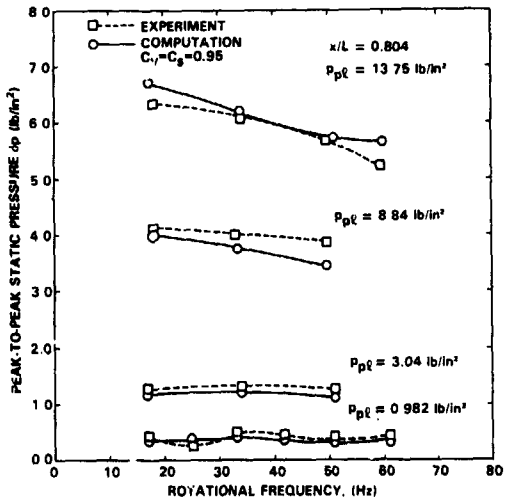

Fig. 8 Peak-to-peak static pressure

presented for two different plenum pressures for both one- and two-per-rev cams. These curves demonstrate the presence of a quarter-wavelength resonance phenomenon in the pipe. This phenomenon is better illustrated in Fig. 9 for the two-per-rev cam where a resonance peak occurs at a frequency of approximately 44 Hz for the numerical solution at the higher pressure and around 55 Hz for the corresponding experimental data. The differences in the resonant frequencies between the numerical and experimental results are likely due to the experiment having a shorter characteristic pipe length because of wave reflection from the end of the nozzle expansion section in the pipe entrance. The quasi-one-dimensional model is unable to simulate this reflection and instead reflects from the pipe entrance itself. It is interesting to note that

the resonance effect is much more pronounced at the higher pressure. For the one-per-rev cam plot shown in Fig. 10, no experimental data were obtained at the expected resonant frequencies of twice the resonant two-per-rev cam frequencies. However, the numerical results again show a resonance at around 75 Hz for the higher pressure and 80 Hz for the lower pressure. These resonant frequencies are somewhat less than twice the two-per-rev cam frequencies. The more pronounced resonant peak for the higher pressure in Fig. 10 is consistent with the two-per-rev cam results.

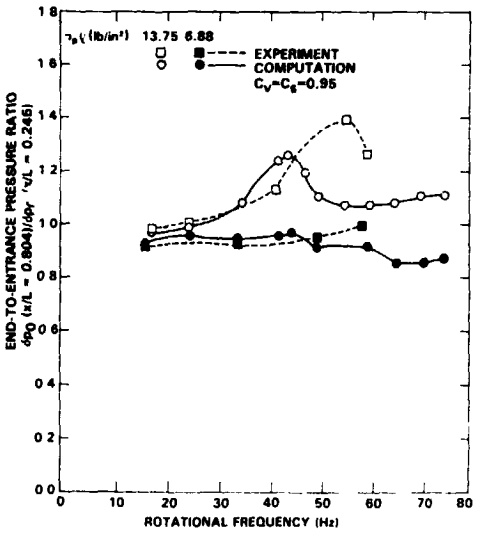

Fig. 9 Resonance phenomenon in pipe; two-per-rev

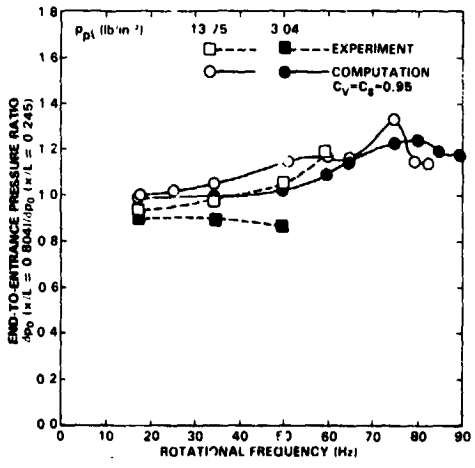

Fig. 10 Resonance phenomenon in pipe; one-per-rev

Effects of Rotational Frequency on Mass Flow Rate

Figures 11 and 12 show the effect of rotational frequency on the computed mean and peak-to-peak mass flow rates, respectively, for the one-per-rev cam at several different plenum pressures. No experimental data are available for comparison with the peak-to-peak data. The experimental lines shown for the mean mass flow rate represent an experimental average since no significant changes in average mass flow rate with frequency were obtained in the experimental data. Likewise very little change was observed in the numerical results.

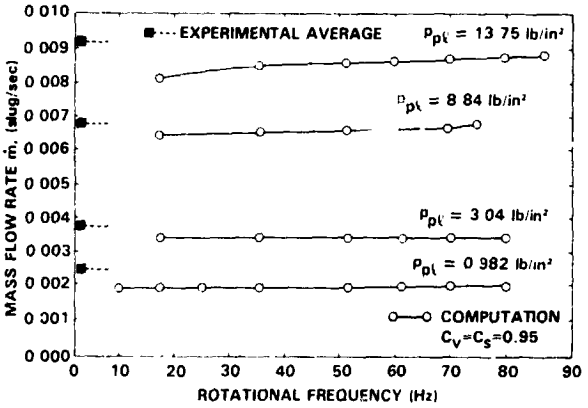

Fig. 11 Mean mass flow rate

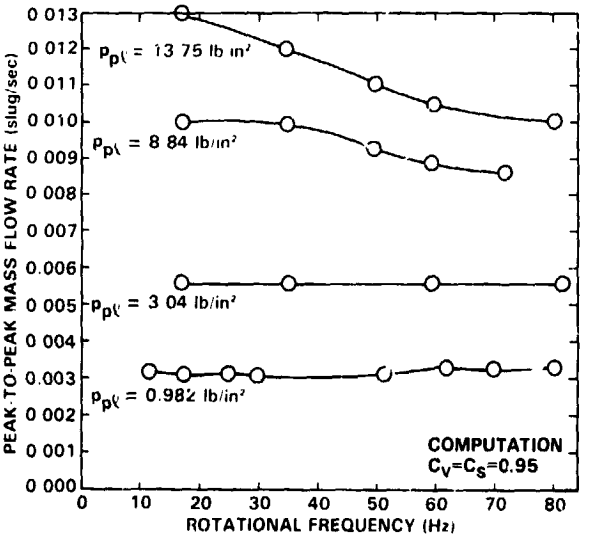

Fig. 12 Peak-to-peak mass flow rate

Figure 13 shows the effect of rotational frequency on the phase of the first harmonic of the mass flow results shown in Figs. 11 and 12. The phase shift increases with increasing plenum pressure (and increasing mass flow rate) and increases almost linearly with frequency over most of the range examined. The linear trend indicates that within this range there is a fixed time delay, almost independent of frequency, associated with a given set of system parameters such as plenum pressure and blade internal geometry. At the higher pressure, capacitance lag is controlling, while at the lower pressure, the lag should be principally sonic lag.

No experimental phase shift data are available for comparison because it is very difficult, if not impossible, to measure dynamic mass flow containing higher harmonics and obtain phase information.

In summary, the comparison of the numerical calculations with experiment, indicate that, even with a simple constant discharge coefficient model, the computer code satisfactorily predicts the system performance over a wide operating range. It is able to predict the trends and magnitudes of the total and static pressures as well as the mass flow rate for plenum pressures from 0.98 to 13.75 psig, for rotational frequencies from 15 to 120 Hz, and for valve area variations from 0 to approximately 1 in.

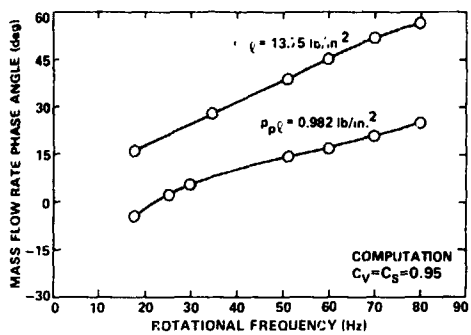

Fig. 13 Mass flow rate phase angle

Theoretical Transient Response

For pneumatic control system design, in addition to a knowledge of the periodic response of the system to periodic control inputs, the transient dynamics are also of interest. In the present study an independent numerical investigation of transient dynamics was conducted. This investigation simulated the pneumodynamic response of the model system to step inputs in control valve settings. This was accomplished by suddenly opening the control valve and allowing air to flow into a blade at atmospheric pressure, allowing steady flow to be established, and then suddenly shutting off the flow, allowing the pressure inside the pipe to return to atmospheric pressure.

The results of this investigation into the system's transient dynamics are shown in Figs. 14 to 17. Figure 14 shows the behavior of the mass flow rate in response to the two control actions for two plenum pressures. The rise or decay time for the mass flow is approximately 0.003 seconds and does not change significantly for the two plenum pressures. This suggests that in these cases the characteristic time phenomena are principally related to the time it takes for a pressure disturbance to propogate the length of the tube, since this is also about 0.003 seconds. This explanation is reinforced by examining Figs. 15 and 16 which are plots of the pressure distribution at various elapsed times after the sudden valve opening. Fig. 15 shows the propagation of the incident pressure wave created by the valve opening and Fig. 16 shows the propagation of the wave after its reflection from the end of the tube. The sonic lag is apparently controlling the transient response to the step input. However, for a system where the capacitance lag is much higher or lower than the sonic lag, the capacitance lag would tend to control the rise or decay. Figure 17 shows the propagation of the incident pressure wave created by sudden valve closing. To smooth these transient results, second-order spatial numerical damping has been added to the numerical algorithm[1] for computing the incremental or "delta" solution for a given time level from the solution for the preceding one. This was done by computing the increment from the weighted average of the second-order (in time) Beam and Warming algorithm and the first-order (in time) algorithm of Lax[5]. The weighting factors applied to the Beam and Warming method and the Lax method were 0.98 and 0.02, respectively.

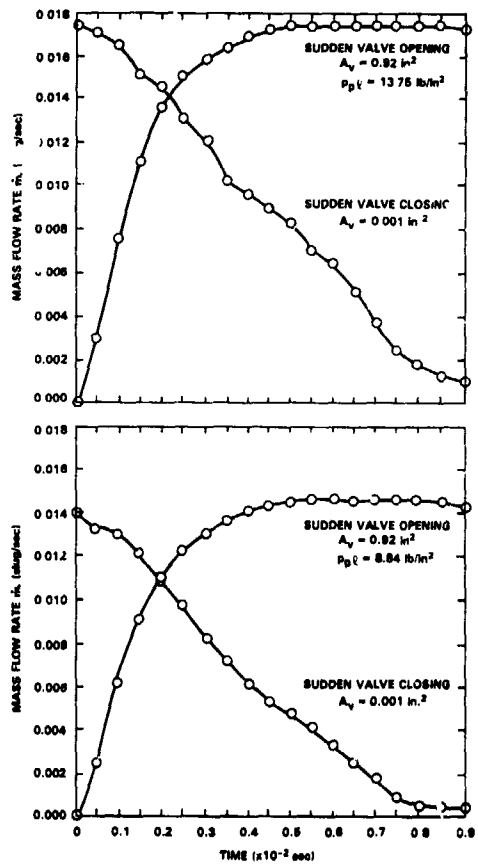

Fig. 14 Theoretical transient mass flow rate

Conclusions

The results presented indicate that quasi-one-dimensional unsteady flow theory can be applied to predict, with reasonable accuracy, the pneumodynamic response of an idealized circulation control rotor model to cyclic control valve inputs.

The results also show that, for a given set of system parameters, the phase lag in the response of the system to cyclic control input is a fixed time delay almost independent of frequency. Higher harmonic content of the mass flow rate output exhibits some amplication due to nonlinear effects, but the higher harmonic content of the pressure response

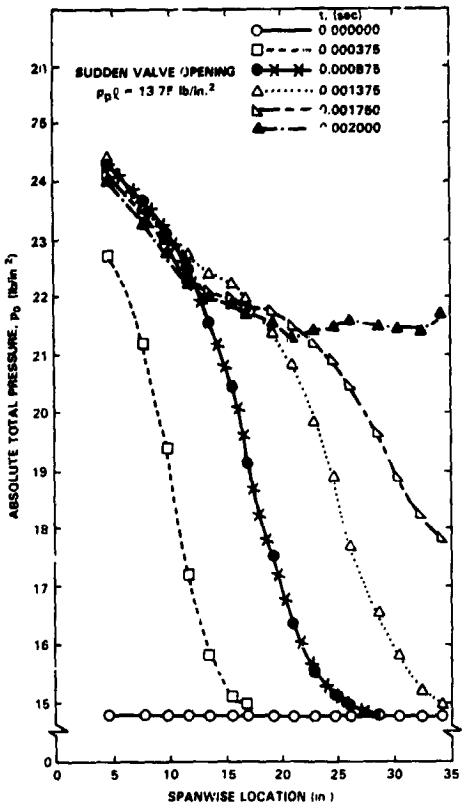

Fig. 15 Theoretical incident transient pressure wave

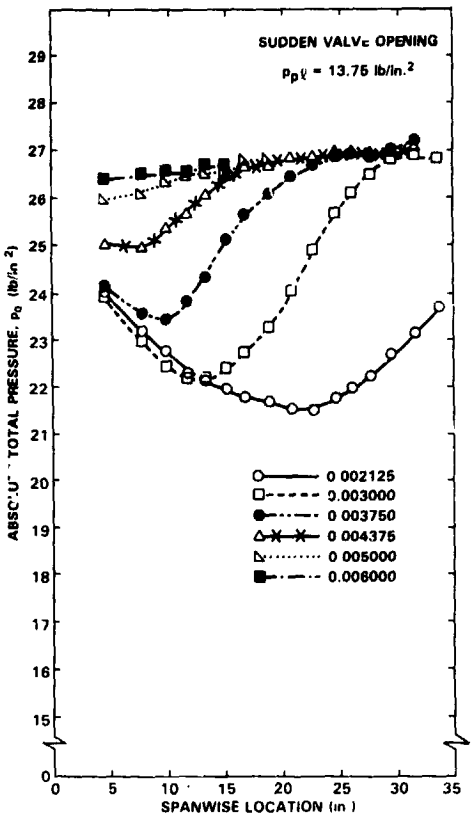

Fig. 16 Theoretical reflected transient pressure wave

does not.

A resonance phenomenon is predicted by the numerical results at approximately the frequency for quarter-wave acoustic resonance in a pipe. The predicted resonant frequencies are slightly different than the experimentally observed resonant frequencies. A possible explanation for this is the inability of the quasi-one-dimensional theory to predict wave reflection from the expansion in the entrance section of the experimental model.

Numerical investigation of the response of the flow variables to step inputs in the control valve area indicate that, for the cases examined, the response time is controlled by the characteristic time for wave propagation (sonic lag).

References

Watkins, C.B., Reader, K.R. and Dutta, S.K., "Numerical and Experimental Simulation of Circulation Control Rotor Pneumodynamics," AIAA Paper No. 83-2551, AIAA/AHS Aircraft Design, Systems and Operations Meeting, Fort Worth, Texas, Oct. 17-19, 1983.

Beam, R.M. and Warming, R.E., "An Implicit Factored Scheme for the Compressible Navier-Stokes Equations," AIAA Journal, Vol. 16, No. 4, pp. 393-402, May 1978.

Reader, K.R., "Evaluation of a Pneumatic Valving System for Application to a Circulation Control Rotor," Naval Ship Research and Development Center Report 4070, May 1973.

Reader, K.R., "The Effects of Cam and Nozzle Configurations on the Performance of a Circulation Control Rotor Pneumatic Valving System," David Taylor Naval Ship Research and Development Center Report ASED-393, Nov. 1977.

Lax, P.D., "Solutions of Nonlinear Hyperbolic Equations and Their Numerical Computation," Communications on Pure and Applied Mathematics, Vol. 7, 1954, pp. 159-193.

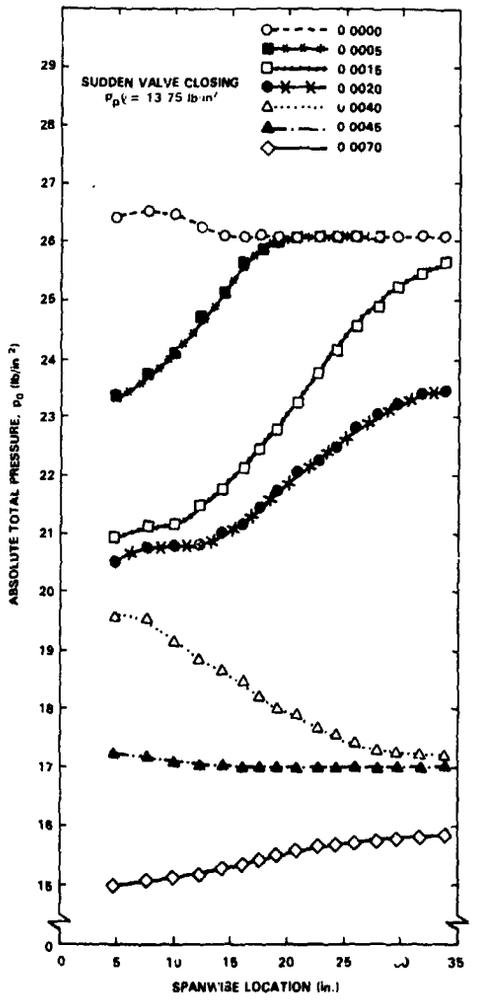

Fig. 17 Theoretical transient pressure wave

DISCUSSION
Paper No. 18

DYNAMIC RESPONSE CHARACTERISTICS OF A CIRCULATION CONTROL ROTOR MODEL PNEUMATIC SYSTEM
Charles B. Watkins
and
Kenneth R. Reader
and
Subash K. Dutta

Andy Lemnios, Kaman Aerospace: First, an observation. On the bench test that we did on the half scale model of the CCR several years ago I believe we observed about a 20 to 30 degree phase lag between the control input to the control valve to the actual buildup of pressure in the plenum chamber. We also observed that the duct of the blade itself charged and discharged as a plenum. Basically there was very little phase lag relationship between the root end of the blade and the tip end of the blade as far as pressure buildups were concerned. Those pressure variations have been documented. I was very pleased to see that in your high freqeuency pneumodynamic analysis you have included flexibility in there. I was wondering if you have any plans to validate the analysis?

Reader: Yes, Andy, over the years we have done that. We've used the H2 data [that] I had to a limited extent. The problem there is that all the tests that we've run so far we've always found we didn't have all the information we needed. In that rotor system we had total pressure at the inboard, [but] the outboard was very questionable. I've had very good results with this code with the H-2 experience, that is, if I look at the components I was able to look at the weight flow, the one per rev and two per rev component at the inboard station and get good correlation if I did a parametric study to identify it. We've looked at the Boeing Vertol data which was tested in Boeing's tunnel about two years ago. We've looked at fixed system results similar to these; half-scale [tests] that were done at UTRC about 3 or 4 years ago. We have not been fortunate enough to get this type of correlation across a large range of parameters, but we can always trace it to some unknown that we haven't been able to measure. One of the big problems we end up with the flexible slots is identifying what that slot area really is. The 25-foot rotor system, we ran correlation with that and we came back to the same position. Most of the time you end up measuring weight flow which goes into all the blades and you have to assume what it is for one blade and then the area variation. I think looking in the box we've worked with most of the data that exists and were fairly reasonable based on engineering level.

Lemnios: Getting back to your comment on the H-2, Ken, the half-scale data I was referring to was the one that was done at Honeywell under a subcontract.

Reader: Yes, I'm aware of that.

Wayne Johnson: I would like to put Andy's question a little bit differently. You describe what you have done in the past and described the capabilities of the analysis that you have. If you were making a list of the things that you didn't know about the duct aerodynamics and that you would really like to know next, where would you start?

Reader: First of all I think the code gives us a good representation analogy. It is a fairly good design tool. The [major] problem is we need more instrumentation on the blades; we need to know more specifics at different radial stations and that is being done.

Johnson: So until you do another round of experiments you really don't know . . .

Reader: That's right. We are using it as a design tool now based on our experiments up to now. The next thing we need is more data. I think we will be getting that, probably in the next year.

Johnson: Since I have the microphone I'm going to ask another question. To make a connection with some of the things we have heard earlier--the dynamic inflow [models] for all their simplicity are extraordinarily useful because they are a discrete state model of the dynamics. I know, at least I think I've seen in some of the earlier work on circulation control rotors that people have developed rather heuristic models of duct aerodynamics, mass-spring type models, which I think they just sort of guessed at Do you think there is a chance that one might start with the kind of model you are using and then use that as a basis for a more solid foundation for a discrete state model for the aerodynamics that then could be a little bit more useful? I think that with a two-dimensional Beam-Warming type solution that you are dealing with fairly significant computation time. I was just wondering if there are ways of that sort that you might go to make a better, but faster model.

Reader: There's one way and it was addressed earlier with Bob Jones' work. If you believe the code then you can regress a model that you need to operate with. But the thing of it is you need to identify all of your parameters up front. There's been some work done on that.

That is, you take the code, you can design a system, get it set up, and then you can linearly regress out of it a faster working model. One of the problems that we have had historically and what has led us to this code is that if you use your analogies to develop [the code] you end up with a lot of constraints on it. Now we had that with the SUPERFLOW code, that is, where we tailored it for specific configurations so that it's good for that specific configuration and it may run a little bit faster--not a whole lot--a little bit, but you ended up without a good design tool. If you go to a real simple model like we had done in the past for stability and control then you end up without the higher harmonic capability. So you end up with two codes and now you have to start keeping track of two codes. I think you are probably better off using a code like this and come up with a regressed model out of it for your actual application.

Bob Wood, Hughes Helicopters: I was interested in your model--the traveling wave [going] down the blade and then reflected back. I didn't really see the thing coming to equilibrium. In other words, is that wave--my question is in several parts, does that wave then come down and then travel back? Essentially, what is the amount of time that's required for a step input before the flow comes to equilibrium?

Watkins: In actuality it's going to reflect back and forth any number of times, but the phenomena tends to be obscured by the flow itself. But essentially it only takes one complete reflection for the flow in the duct to pretty much distribute itself evenly over the length.

Reader: I'd just like to make a comment on Wayne's question just a minute ago. I just had another thought. One thing that we found, for instance right now, to do this work we've run 16 elements in it and it has taken the cost up for running the code. However, if you back off the number of elements, depending upon what you are using it for, you may not need the fidelity, so if you back off the elements your time goes way down--probably a factor of 4 to maybe 5 depending upon the number of elements. Kaman did some of that work earlier with their codes and they found that, for instance, for some cases they needed 4 to 6 elements, but for general handling quality-type stuff they only needed one. I think that is what Andy was alluding to earlier. Depending upon what you are doing with the pneumodynamics and what you need out of it--if you only need one per rev cyclic in order to do stability and control you can come up with a fairly simple model for that.